

# Tough and Self-Healing Hydrogels Formed via Hydrophobic Interactions

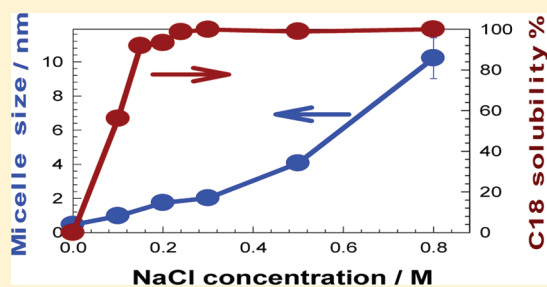
Deniz C. Tuncaboylu,<sup>†</sup> Murat Sari,<sup>†</sup> Wilhelm Oppermann,<sup>\*,‡</sup> and Oguz Okay<sup>\*,†</sup>

<sup>†</sup>Department of Chemistry, Istanbul Technical University, 34469 Maslak, Istanbul, Turkey

<sup>‡</sup>Institute of Physical Chemistry, Clausthal University of Technology, Arnold-Sommerfeld-Strasse 4, 38678 Clausthal-Zellerfeld, Germany

**S** Supporting Information

**ABSTRACT:** Large hydrophobic monomers stearyl methacrylate (C18) and dococyl acrylate (C22) could be copolymerized with the hydrophilic monomer acrylamide in a micellar solution of sodium dodecyl sulfate (SDS). This was achieved by the addition of salt (NaCl) into the reaction solution. Salt leads to micellar growth and, hence, solubilization of the hydrophobes within the SDS micelles. The hydrogels thus obtained without a chemical cross-linker exhibit unique properties due to the strong hydrophobic interactions. They can only be dissolved in SDS solutions demonstrating the physical nature of cross-links. Results of dynamic light scattering, rheological and mechanical measurements show that the hydrophobic associations between the blocks of C18 or C22 units prevent water solubility and flow, while the dynamic nature of the junction zones provides homogeneity and self-healing properties together with a high degree of toughness. When fractured, the hydrogels formed using C18 associations can be repaired by bringing together fractured surfaces to self-heal at room temperature, after which, they again exhibit the original extensibility of about 3600%. The existence of free, nonassociated blocks in C18 hydrogels is accounted for their high self-healing efficiencies.



## INTRODUCTION

Self-healing is one of the most remarkable properties of biological materials such as skin, bones, and wood.<sup>1,2</sup> The special ability of natural materials to heal cracks often involves an energy dissipation mechanism due to the so-called sacrificial bonds that break and reform dynamically before the fracture of the molecular backbone.<sup>3</sup> Although synthetic hydrogels are very similar to biological tissues, they are normally very brittle and lack the ability to self-heal, which hinders their use in any stress-bearing applications. Numerous studies have been conducted in recent years to improve the mechanical performance of hydrogels formed by free-radical cross-linking copolymerization.<sup>4–10</sup>

The poor mechanical performance of chemically cross-linked hydrogels mainly originates from their very low resistance to crack propagation due to the lack of an efficient energy dissipation mechanism in the gel network.<sup>11,12</sup> To obtain a gel with a high degree of toughness, one has to increase the overall viscoelastic dissipation by creating a polymer network where cross-linking occurs via reversible breakable cross-links with finite lifetimes, instead of permanent cross-links.<sup>13</sup> Design of self-healing materials capable of recovering their original mechanical performance after fracture also requires intermolecular noncovalent interactions.<sup>10,14–17</sup> It was shown that a rubber-like material formed via hydrogen bonds self-heals due to the hydrogen bond-forming groups located in excess at the fractured surfaces so that healing can be induced by pressing these surfaces together.<sup>14</sup>

Hydrophobic interactions play a dominant role in the formation of large biological systems. These interactions can be generated in synthetic hydrogels by incorporation of hydrophobic sequences within the hydrophilic polymer network chains.<sup>18</sup> Recently, we have shown that hydrogels formed by hydrophobic associations exhibit a high degree of toughness due to the mobility of the junction zones within the gel network, which contributes to the dissipation of the crack energy along the hydrogel sample.<sup>13</sup> Hydrophobically modified hydrogels were prepared by copolymerization of the hydrophilic monomer acrylamide (AAM) in the presence of a small amount of a hydrophobic comonomer via micellar polymerization technique. In this technique, a water insoluble hydrophobic comonomer solubilized within the micelles is copolymerized with a hydrophilic monomer in aqueous solutions by free-radical addition polymerization.<sup>19–26</sup> Because of high local concentration of the hydrophobe within the micelles, the hydrophobic monomers are distributed as random blocks along the hydrophilic polymer backbone. It was shown that *n*-alkylacrylamides or *n*-alkyl methacrylates with an alkyl chains length between 4 and 12 carbon atoms can easily be copolymerized with AAM to obtain tough hydrogels.<sup>13,27</sup> However, larger hydrophobes such as stearyl methacrylate (C18) or dococyl acrylate (C22) cannot be copolymerized with AAM simply

Received: March 14, 2011

Revised: May 23, 2011

Published: June 02, 2011

in a micellar solution of sodium dodecyl sulfate (SDS). This is due to the very low water solubility of these monomers (e.g.,  $10^{-9}$  mL/mL for C18<sup>28</sup>), which restricts the monomer transport through the continuous aqueous phase into the micelles.<sup>29,30</sup> Incorporation of blocks of large hydrophobes into the polyacrylamide backbone would produce strong and long-lived hydrophobic associations making self-healing efficient.

It has been known for a long time that the addition of electrolyte into aqueous ionic surfactant solutions weakens electrostatic interaction and causes the micelles to grow.<sup>31,32</sup> The micellar structure changes from sphere to rod and then, to large cylindrical aggregates or flexible worm-like micelles.<sup>32</sup> The worm-like micelles are similar to polymers in that they are quite flexible, while they differ from classical polymers in that they are constantly breaking and forming.<sup>33</sup> The sphere-to-rod growth in the SDS micelles occurs by the addition of inorganic or organic salts.<sup>34–39</sup> Spherical SDS micelles of radius 2.5 nm grow significantly bigger at NaCl concentrations above 0.45 M.<sup>40</sup> For example, the micelle aggregation number increases from about 80 in 0.15 M NaCl to about 1000 in 0.60 M NaCl at 25 °C.<sup>34</sup> It is also known that solutions of rodlike micelles can solubilize rather large amounts of hydrocarbons, whereupon they transform into large spherical micelles for thermodynamic feasibility.<sup>41–44</sup>

Here, we show, for the first time to our knowledge, that acrylamide can be copolymerized with large hydrophobes such as C18 or C22 in a micellar system provided that an electrolyte, such as NaCl, has been added in sufficient amount. As will be seen below, the hydrogels thus obtained without a chemical cross-linker exhibit unique properties. Strong hydrophobic associations between the blocks of C18 or C22 prevent dissolution in water and flow, while the dynamic nature of the junction zones between the network chains provides self-healing properties together with a high degree of toughness.

## EXPERIMENTAL PART

**Materials.** Acrylamide (AAm, Merck), *N,N'*-methylenebis(acrylamide) (BAAm, Merck), sodium dodecyl sulfate (SDS, Sigma), ammonium persulfate (APS, Merck), *N,N,N',N'*-tetramethylethylenediamine (TEMED, Merck), and NaCl (Merck) were used as received. Commercially available stearyl methacrylate (C18, Fluka) used in the present work as one of the hydrophobic monomers consists of 65% *n*-octadecyl methacrylate and 35% *n*-hexadecyl methacrylate. The other hydrophobic comonomer dococyl acrylate (C22) was prepared by the reaction of the 1-docosanol with acryloyl chloride in THF in the presence of triethylamine as a catalyst, as described in the literature.<sup>45</sup> The purity of each batch of C22 was checked by NMR, FTIR, and elemental analysis. An APS stock solution was prepared by dissolving 0.8 g of APS in 10 mL of distilled water.

**Hydrogel Preparation.** Micellar copolymerization of AAm with C18 or with C22 was conducted at 25 °C in the presence of an APS (3.5 mM)–TEMED (0.25 v/v %) redox initiator system. Following parameters were fixed:

- Total monomer (acrylamide + C18 or C22) concentration: 5 w/v %
- Hydrophobe content of the monomer mixture: 2 mol %
- SDS concentration: 7 w/v %

To illustrate the synthetic procedure, we give details for the preparation of hydrogels in 0.8 M NaCl solution: SDS (0.7 g) was dissolved in 9.9 mL of 0.8 M NaCl at 35 °C to obtain a transparent solution. Then, C18 (0.0430 g) was dissolved in this SDS–NaCl solution under stirring for 2 h at 35 °C. After addition and dissolving acrylamide (0.457 g) for 30 min, TEMED (25  $\mu$ L) was added into the solution. Finally, 0.1 mL of APS stock solution was added to initiate the reaction. For the rheological experiments, a portion of this solution was transferred between the

plates of the rheometer. For the determination of the gel fraction and for the mechanical measurements, the remaining part of the solution was transferred into several plastic syringes of 4 mm internal diameters and the polymerization was conducted for 1 day at 25 °C. For the dynamic light scattering measurements, the solution was filtered through Nylon membrane filters with a pore size of 0.2  $\mu$ m into light scattering vials.

**Quantification of the Solubilization of C18 in the Reaction Solution.** The amount of C18 solubilized in the micelles of the reaction solution was estimated by static light scattering measurements performed on gels made without filtration of the solution, in comparison to those obtained after filtration. For this purpose, we used a multiangle light scattering DAWN EOS (Wyatt Technologies Corporation) equipped with a vertically polarized 30 mW gallium–arsenide laser operating at  $\lambda = 690$  nm. Prior to the addition of the initiator APS, each reaction solution was divided in two portions. One part was filtered through a membrane filter with a pore size of 0.45  $\mu$ m while the other part was not filtered. After 1 day of reaction time, the scattering intensities were measured at a scattering angle of 90°. It was presumed that undissolved/unsolubilized C18 causes strong scattering, while filtration removes this undissolved material and the scattering intensity is reduced correspondingly. The solubilization extent of C18 ( $s$  %) was calculated as:  $S \% = 10^2 (1 - \Delta R_q / \Delta R_{q,0})$ , where  $\Delta R_q$  and  $\Delta R_{q,0}$  are the differences of the scattered intensities between unfiltered and filtered solutions at a given salt concentration  $C_{salt}$  and at  $C_{salt} = 0$ , respectively.  $s$  % was also determined by measuring the transmittance of SDS–NaCl solutions containing various amounts of C18 on a T80 UV–visible spectrophotometer. The transmittance at 500 nm was plotted as a function of the added amount of C18 in the SDS–NaCl solution and, the solubilization extent of C18 was determined by the curve break.

**Rheological Experiments.** Gelation reactions were carried out within the rheometer (Gemini 150 Rheometer system, Bohlin Instruments) equipped with a cone-and-plate geometry with a cone angle of 4° and diameter of 40 mm. The instrument was equipped with a Peltier device for temperature control. During all rheological measurements, a solvent trap was used to minimize the evaporation. A frequency of 1 Hz (corresponding to an angular frequency  $\omega = 6.3$  rad/s) and a deformation amplitude  $\gamma_o = 0.01$  were selected to ensure that the oscillatory deformation is within the linear regime. The reactions were monitored in the rheometer at 25 °C up to a reaction time of about 3 h. After 3 h, frequency-sweep tests at  $\gamma_o = 0.01$  were carried out at 25 °C over the frequency range 0.01 to 40 Hz (0.063–250 rad/s). The gels formed within the rheometer were also subjected to stress-relaxation experiments at 25 °C. A constant shear deformation  $\gamma_o$  was applied to the gel samples in a stepwise manner and the resulting stress  $\sigma(t, \gamma_o)$  was monitored as a function of time. Such experiments were conducted with increasing strains  $\gamma_o$  ranging from 0.01 to 100. For each gel, stress-relaxation experiments at various  $\gamma_o$  were conducted starting from a value of the relaxation modulus deviating less than 10% from the modulus measured at  $\gamma_o = 0.01$ .

**Dynamic Light Scattering (DLS) Measurements.** DLS measurements on SDS–NaCl solutions with and without the monomers C18 and AAm were performed in the instrument Zetasizer Nano S from Malvern. The instrument contains a 4 mW He–Ne laser operating at a wavelength  $\lambda$  of 633 nm with a fixed detector angle of 173° and incorporates noninvasive backscatter optics. The measurements were performed at both 35 and 25 °C, which are the solubilization temperature of C18 in SDS–NaCl solution and the reaction temperature, respectively. The data were analyzed by the cumulant method using Malvern application software, and the hydrodynamic correlation lengths  $\xi_H$  were obtained from the first cumulant.

DLS measurements on hydrogels were performed at 25 °C after a reaction time of 24 h using ALV/CGS-3 compact goniometer (ALV, Langen, Germany) equipped with a cuvette rotation/translation unit (CRTU) and a He–Ne laser (22 mW,  $\lambda = 632.8$  nm). The scattering

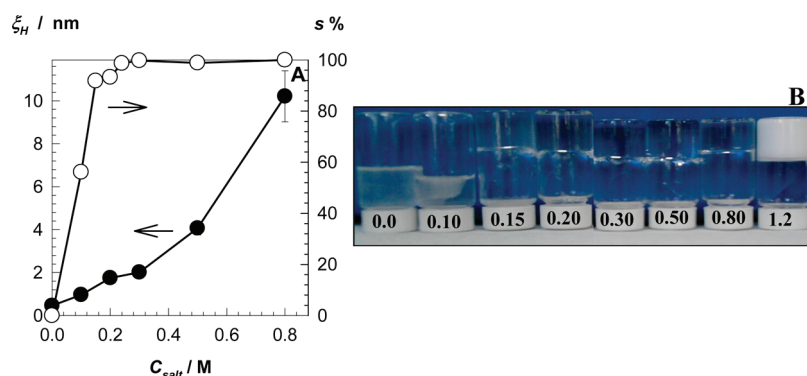


**Figure 1.** (A) Hydrodynamic correlation length  $\xi_H$  of SDS solutions at 35 °C (●), and the solubilization extent of C18,  $s$  % (○) shown as a function of  $C_{salt}$ . (B) Images of the reaction solutions in inverted glass vials after 1 day of the reaction time.  $C_{salt}$  (in M) as indicated.

angle  $\theta$  was fixed to be 90° which corresponds to the scattering vector  $q = 1.87 \times 10^7 \text{ m}^{-1}$ , where  $q = (4\pi n/\lambda) \sin(\theta/2)$ ,  $n$  the refractive index of the solvent. A fiber optical detection unit based on three-mode detection was used, which includes an appropriate collimator/GRIN-lens fiber and the ALV/STATIC and DYNAMIC enhancer. To protect the detector, the intensity of the incident light is automatically attenuated at each measurement by an eight-step automatic software-controlled attenuator and measured with a monitor diode. Thus, the intensity of incident light can be different within a series of measurements. When discussing scattering intensities, we therefore use data that were rescaled to a preset value of the monitor diode assuming a linear count rate dependence. Toluene was used as the index matching liquid. The temperature was controlled with an external thermostat. The time averaged intensity correlation functions were acquired at 100 different sample positions selected by randomly moving the CRTU before each run. The acquisition time for each run was 30 s.

DLS provides the time average intensity correlation function  $g_T^{(2)}(q, \tau)$ , defined as<sup>46</sup>

$$g_T^{(2)}(q, \tau) = \frac{\langle I(q, 0)I(q, \tau) \rangle_T}{\langle I(q, 0) \rangle_T^2} \quad (1)$$

whose short-time limit can be related to an apparent diffusion coefficient,  $D_A$ , via:<sup>46,47</sup>

$$D_A = -\frac{1}{2q^2} \lim_{\tau \rightarrow 0} \frac{d(\ln(g_T^{(2)}(q, \tau) - 1))}{d\tau} \quad (2)$$

where  $\tau$  is the decay time, and  $\langle \dots \rangle_T$  denotes time average. For a nonergodic medium like polymer gels,  $D_A$  and likewise, the time-averaged scattering intensity  $\langle I(q) \rangle_T$  varies randomly with sample position.  $\langle I(q) \rangle_T$  has two contributions, one from static inhomogeneities (frozen structure) and the other from dynamic fluctuations according to the following equation:<sup>46–48</sup>

$$\langle I(q) \rangle_T = I_C(q) + \langle I_F(q) \rangle_T \quad (3)$$

Here  $I_C(q)$  and  $\langle I_F(q) \rangle_T$  are the scattered intensities due to the frozen structure and liquidlike concentration fluctuations, respectively. To separate  $\langle I(q) \rangle_T$  into its two parts, we follow the method proposed by Joosten et al.<sup>46</sup> Treating the system by the partial heterodyne approach, one obtains

$$\frac{\langle I(q) \rangle_T}{D_A} = \frac{2\langle I(q) \rangle_T}{D} - \frac{\langle I_F(q) \rangle_T}{D} \quad (4)$$

The cooperative diffusion coefficient  $D$  and the fluctuating component of the scattering intensity  $\langle I_F(q) \rangle_T$  of the present hydrogels were obtained by plotting  $\langle I(q) \rangle_T / D_A$  vs  $\langle I(q) \rangle_T$  data recorded at 100 different sample positions (Figure S1, Supporting information). The dynamic correlation length  $\xi$  was evaluated by  $\xi = kT / (6\pi\eta D)$ , where  $\eta$  is the viscosity of the medium (0.89 mPa·s) and  $kT$  is the Boltzmann energy.

**Gel Fractions and Swelling Measurements.** After polymerization in syringes, hydrogel samples were immersed in a large excess of water at 24 °C for at least 30 days by replacing water every second or third day to extract any soluble species. SDS concentration in the external solutions was estimated using the methylene blue method.<sup>49</sup> The masses  $m$  of the gel samples were monitored as a function of swelling time by weighing the samples. Relative weight swelling ratio  $m_{rel}$  of gels was calculated as  $m_{rel} = m/m_0$ , where  $m_0$  is the initial mass of the gel sample. Then, the equilibrium swollen gel samples were taken out of water and immersed in liquid nitrogen for 5 min before they were freeze-dried. The gel fraction  $W_g$ , that is, the conversion of monomers to the cross-linked polymer (mass of cross-linked polymer/initial mass of the monomer) was calculated from the masses of dry, extracted polymer network and from the comonomer feed. Swelling measurements in aqueous NaCl or SDS solutions were also carried out as described above, except that the mass of the hydrogel sample and the volume of external solution were fixed at 1.0 g and 100 mL, respectively, and the solutions were refreshed every day. The polymers dissolved in SDS solutions were precipitated by adding the solutions into an excess of methanol and the precipitate was dried under vacuum. FTIR spectra of the polymers were recorded on a Perkin-Elmer FT-IR Spectrum One-B spectrometer. Since the polymers could only be dissolved in rather concentrated SDS solutions, a (highly desirable) molecular characterization with regards to molecular weight, block length, etc. could not be achieved.

**Uniaxial Compression Measurements.** The measurements were performed on equilibrium swollen hydrogels. All the mechanical measurements were conducted in a thermostated room at  $24 \pm 0.5$  °C. The stress–strain isotherms were measured by using an apparatus previously described by our group.<sup>50</sup> The elastic modulus  $G_{swollen}$  was determined from the slope of the linear dependence  $f = G_{swollen}(\alpha - \alpha^{-2})$ , where  $f$  is the force acting per unit cross-sectional area of the undeformed gel specimen, and  $\alpha$  is the deformation ratio (deformed length/initial length).

**Uniaxial Elongation Measurements.** The measurements were performed on cylindrical hydrogel samples in the state of preparation (4 mm diameter  $\times$  50 mm length) and after equilibrium swelling in water using a Zwick Roell, 10 N test machine at 25 °C under the following conditions: crosshead speed = 50 mm/min, sample length between jaws = 20 mm. The tensile strength (from the initial cross section of  $12.57 \text{ mm}^2$ ) and percentage elongation at break were recorded. For reproducibility, at least six samples were measured for each gel and the results were averaged.

## RESULTS AND DISCUSSION

In the following, we will mainly discuss the results obtained using stearyl methacrylate C18 as the hydrophobic comonomer of acrylamide (AAM). The micellar copolymerization of AAM

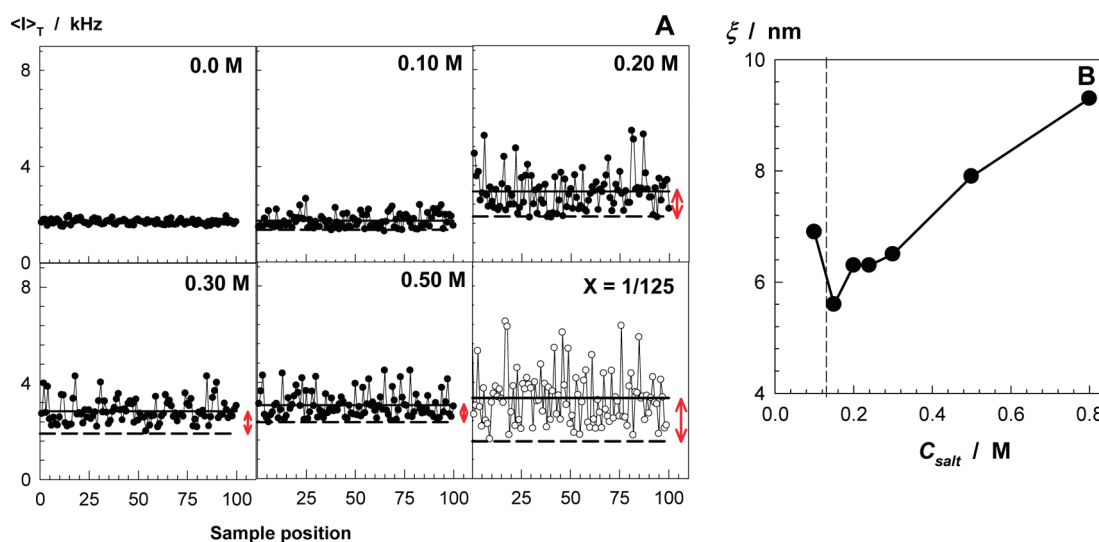


**Figure 2.** (A) Variation of  $\langle I \rangle_T$  with the sample position for reaction solutions at various  $C_{salt}$  indicated. The figure in the bottom right is for a chemical PAAm hydrogel ( $X = 1/125$ ). (B) Dynamic correlation length  $\xi$  plotted against  $C_{salt}$ . The dashed line indicates the minimum salt concentration required for gel formation.

with 2 mol % C18 was carried out at various NaCl concentrations  $C_{salt}$ . SDS concentration was fixed at 7 w/v %, which is much above the overlap concentration of SDS micelles.<sup>51</sup> The last paragraph will then summarize the specific features of the gels formed using dococyl acrylate C22 comonomer.

**Solubilization of C18 in SDS Micelles.** The major synthetic challenge consists of creating suitable conditions so that adequate amounts of large hydrophobes, such as C18 or C22 having very poor water solubility, can be solubilized. It was found that the addition of salt into micellar SDS solutions provides solubilization of these hydrophobes and thus permits their copolymerization with AAm in aqueous media. Figure 1A demonstrates the salt-induced solubilization of C18 in an aqueous SDS solution (7 w/v %). The solubilization extent of C18 ( $s\%$ ) is plotted against NaCl concentration,  $C_{salt}$ , and also the hydrodynamic correlation length,  $\xi_H$ , of these solutions is shown. As  $C_{salt}$  is increased,  $\xi_H$  increases first slowly and then rapidly above  $C_{salt} = 0.3$  M, clearly indicating that the micelles grow bigger. If one assumes a prolate ellipsoidal shape for SDS micelles in aqueous NaCl and equates the semimajor axis with the radius of the minimum spherical micelle (2.5 nm),<sup>34,36</sup> one may estimate the semimajor axis of the micelles using Perrin's equations.<sup>52,53</sup> Such calculations show that, at  $C_{salt} = 0.5$  and 0.8 M, the major axis between the entanglements becomes 8 and 34 nm, respectively, with corresponding aggregation numbers 200 and 800, as compared to 60 for the minimum spherical SDS micelle. Open symbols in Figure 1A showing the solubilization extent of C18 in the reaction solution reveal that the growth of SDS micelles with rising salt concentration is accompanied by enhanced solubilization of C18, and complete solubilization (0.48 w/v %) occurs at 0.3 M NaCl and above.

We have to mention that, after addition of C18 and AAm into the micellar solution, the hydrodynamic correlation length  $\xi_H$  decreased again due to the oil-induced structural change of wormlike micelles, as has been reported for several surfactant systems (Figure S2, Supporting Information).<sup>41–44,54</sup> Even visual inspection of the solutions provided evidence that the solubilization of C18 reduces the viscosity of SDS–NaCl solutions. This change likely occurs due to the accumulation of the

monomers in the surfactant palisade layer and in the core of micelles, which increases the curvature of the micelle making rod–sphere transition in micellar shape favorable.

**Formation of Physical Gels.** After addition of the monomers and the initiator into the micellar solution and, after the copolymerization reactions, physical gels were obtained in the range of  $C_{salt}$  between 0.15 and 3 M. Figure 1B shows the optical images of the reaction solutions in inverted vials after 1 day of the reaction time. No gel forms in the absence of NaCl and a turbid polymer solution was obtained due to the insolubility of the hydrophobic comonomer in SDS solution. The gel starts to form above 0.1 M NaCl; simultaneously, the turbidity decreases as  $C_{salt}$  is increased. Transparent gels were obtained in the range of  $C_{salt}$  between 0.3 and 0.8 M due to the complete solubilization of C18 in the SDS micelles. At larger salt contents, although the initial reaction solutions were transparent, opaque gels or solutions ( $C_{salt} \geq 3.0$ ) were obtained after the polymerization suggesting that a phase separation occurs during the course of the reactions due to the aggregation of micelles.<sup>40</sup> In the following, salt concentrations in the reaction solutions were limited below 1 M NaCl to obtain transparent hydrogels.

Gel formation could be simply recognized by observing speckles, i.e., random fluctuations in the intensity of scattered light as a function of sampling position, when performing dynamic light scattering measurements. Figure 2A shows the variations of time-averaged scattering intensity  $\langle I \rangle_T$  with randomly chosen sample position for gels formed by micellar copolymerization at various  $C_{salt}$  (after 24 h of reaction time). Note that the reaction solutions were filtered before the addition of the initiator to eliminate the effect of undissolved C18 at low salt contents. In comparison, the lower right panel shows the data obtained for a polyacrylamide (PAAm) hydrogel prepared using a chemical cross-linker (BAAm) at a cross-linker ratio  $X = 1/125$  (molar ratio of BAAm to the monomer AAm). The chemical gel was prepared at the same monomer concentration as the physical gels made by micellar copolymerization, and it exhibits a comparable modulus of elasticity, i.e., 1.1 kPa at 1 Hz. The solid lines in the figures represent the ensemble-averaged scattering intensity,  $\langle I \rangle_E$ , obtained by averaging  $\langle I \rangle_T$  over all sample

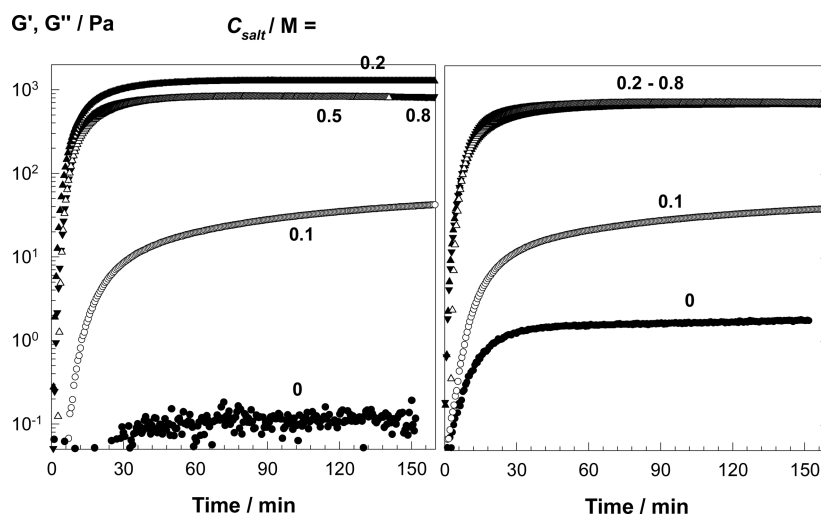


**Figure 3.** Elastic modulus  $G'$  (left) and viscous modulus  $G''$  (right) during the micellar copolymerization of AAm and C18 shown as a function of the reaction time.  $C_{\text{salt}} = 0$  (●), 0.1 (○), 0.2 (▲), 0.5 (△), and 0.8 (▼).  $\omega = 6.3$  rad/s,  $\gamma_o = 0.01$ .

positions. As expected,  $\langle I \rangle_T = \langle I \rangle_E$  for  $C_{\text{salt}} = 0$  M due to the formation of a PAAm solution which is an ergodic medium. By increasing the salt concentration above 0.1 M, spatial fluctuations in  $\langle I \rangle_T$  appear, indicating that the system has become a non-ergodic medium, a gel. This parallels closely the macroscopic behavior as seen in Figure 1B, and it supports the notion that a minimum salt concentration around 0.15 M is necessary to solubilize enough C18 in order to achieve cross-linking of the polymer chains via blocks of hydrophobic moieties.

The dashed lines in Figure 2A represent that part of the scattering intensities  $\langle I_F \rangle_T$  which is due to liquidlike concentration fluctuations.  $\langle I_F \rangle_T$  monotonically increases with  $C_{\text{salt}}$  and its magnitude at high salt contents is larger than that in chemical hydrogels of the same polymer concentration. This is attributed to the fact that an appreciable portion of the thermal scattering in these gels is due to the presence of large SDS micelles. Moreover, the frozen component  $I_C$  of the scattered intensity, represented by the height of the double arrows in Figure 2A, decreases with increasing  $C_{\text{salt}}$  from 0.2 to 0.5 M indicating an increasing degree of homogeneity of the physical gels. Figure 2A also shows that the gels formed by the associations of C18 blocks are more homogeneous than the corresponding chemical PAAm hydrogel. Stated otherwise, the inhomogeneity is suppressed due to the reversible nature of the cross-linkages. This is in accord with previous reports showing that the incorporation of mobile cross-link zones into a gel network reduces the spatial gel inhomogeneity.<sup>55,56</sup>

The time average intensity correlation functions exhibit two relaxation modes: a major fast one at several 10  $\mu$ s and a minor slow one around 1 s (Figure S3, Supporting Information). We calculated the dynamic correlation length  $\xi$  on the basis of the fast mode. In Figure 2B,  $\xi$  is plotted against  $C_{\text{salt}}$ . ( $\xi$  was computed from  $D$  as obtained by eq 4 when there was an appreciable speckle pattern, at  $C_{\text{salt}} \geq 0.15$  M, or just from the arithmetic average of  $D_A$  for ergodic solutions, at  $C_{\text{salt}} < 0.15$  M. The dashed line in the figure indicates the minimum salt concentration required for gel formation.)  $\xi$  of the physical gels is slightly increasing with rising  $C_{\text{salt}}$ . It is in the same range as that of chemical gels.<sup>57</sup> Since the elastic modulus and thus, the effective cross-link density of the gels does not change much over the whole range of  $C_{\text{salt}}$  (see below), the increase of  $\xi$  is

probably related to the increasing size of the micelles or the increasing size of intermolecular hydrophobic associations in the gel network. We expect the slow mode to indicate the clusters (hydrophobic associations, surfactant agglomerates) within the network, on the spatial scale of  $1/q$ .

The copolymerization reactions of AAm and C18 in micellar solutions were also monitored by rheometry using oscillatory deformation tests. Figure 3 shows the elastic modulus  $G'$  (left) and viscous modulus  $G''$  (right) plotted against the reaction time at various  $C_{\text{salt}}$ . In the absence of NaCl, the dynamic modulus vs time profile of the reaction system is similar to that of the micellar polymerization of AAm alone. In the presence of NaCl, both moduli increase rapidly and then approach plateau values after 1–2 h (for  $C_{\text{salt}} > 0.1$  M). The addition of just 0.1 M NaCl into the reaction solution already leads to a marked increase of both  $G'$  and  $G''$ , demonstrating gel formation by incorporation of the hydrophobic blocks into the PAAm chains and formation of intermolecular associations.

Figure 4A shows the limiting values of  $G'$  (filled circles),  $G''$  (open circles), and the loss factor  $\tan \delta$  (squares) after completion of the reaction as a function of  $C_{\text{salt}}$ . Both  $G'$  and  $G''$  increase steeply when  $C_{\text{salt}}$  rises from 0 to 0.2 M, while, they do not change much between  $C_{\text{salt}} = 0.2$  and 0.8 M, and hydrogels with  $G'$  around 1 kPa and a loss factor of 0.5–0.9 were obtained. Figure 4B shows the frequency dependences of  $G'$  (filled symbols) and  $G''$  (open symbols) for the gels formed at various salt contents. The data are vertically shifted by one or several decades to avoid overlapping. At  $C_{\text{salt}} = 0.10$  M, the system shows a liquidlike response typical for a semidilute polymer solution, i.e.  $G''$  exceeds  $G'$  at low frequencies and there is a crossover between  $G'$  and  $G''$  at 3.8 rad/s. The crossover frequency shifts toward lower values as  $C_{\text{salt}}$  is increased and at  $C_{\text{salt}} = 0.24$  M, it shifts outside of the experimental window. Between  $C_{\text{salt}} = 0.24$ –0.80 M,  $G'$  is always slightly higher than  $G''$  in the whole frequency range with a plateau appearing in the  $G'$  vs  $\omega$  curve at high frequencies. At frequencies below 3 rad/s, both  $G'$  and  $G''$  are congruent and show power-law behavior,  $G' \propto \omega^{0.46 \pm 0.03}$ ,  $G'' \propto \omega^{0.44 \pm 0.01}$  suggesting that the gels are close to the critical gel state possessing self-similar fractal structure over a wide spatial scale. According to Winter and Chambon, the frequency independence of  $\tan \delta$  provides a convenient method to determine the gel point and

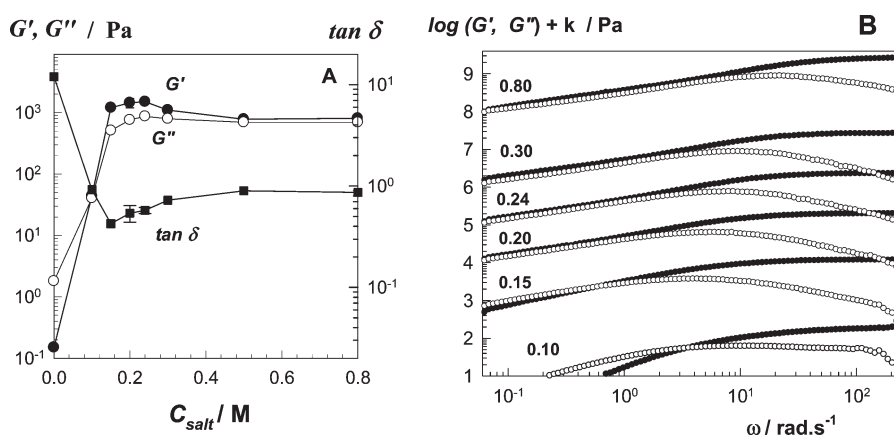


**Figure 4.** A: The limiting values of  $G'$  (filled circles),  $G''$  (open circles), and the loss factor  $\tan \delta$  (squares) plotted against  $C_{salt}$ .  $\omega = 6.3$  rad/s,  $\gamma_o = 0.01$ . B:  $G'$  (filled symbols) and  $G''$  (open symbols) shown as a function of angular frequency  $\omega$  measured after 3 h of reaction time.  $k$  is a shift factor to avoid overlapping.  $k = 0, 1, 2, 3, 4,$  and  $6$  with increasing  $C_{salt}$  indicated.

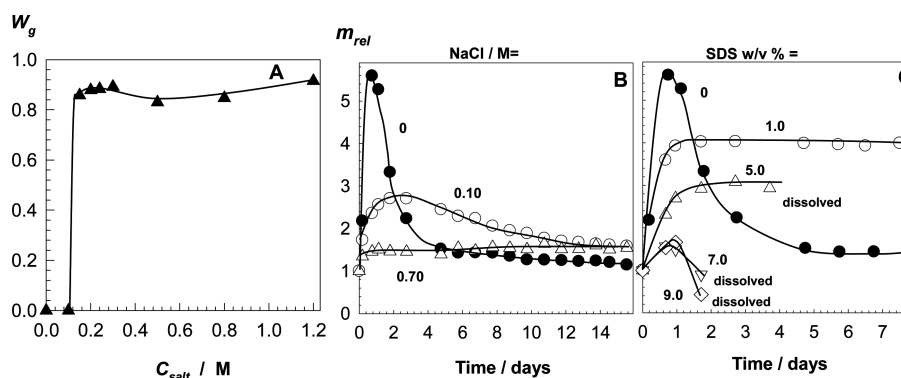


**Figure 5.** (A) Gel fraction  $W_g$  shown as a function of  $C_{salt}$ . (B, C) Relative weight swelling ratio  $m_{rel}$  of C18 hydrogels prepared in 0.5 M NaCl in aqueous solutions of NaCl (B) and SDS (C) shown as a function of the swelling time. NaCl and SDS concentrations in the external solutions are indicated.

the critical exponent.<sup>58,59</sup> For the present hydrogels, the critical salt concentration at which  $\tan \delta$  at frequencies below 4 rad/s overlaps is 0.24 M NaCl yielding a critical exponent of 0.46, which is in good agreement with the Kramers–Kronig relation for a gel network at the sol–gel transition.<sup>58</sup>

**Swelling Behavior of Physical Gels and Their Solubilization in SDS Solutions.** The physical gels formed using hydrophobic associations were insoluble in water. Results of the gel fraction  $W_g$  measurements (mass of dry, extracted network/mass of the monomers in the comonomer feed) shown in Figure 5A reveal that a NaCl concentration of 0.15 M is required for the formation of insoluble gels.  $W_g$  equals  $0.86 \pm 0.04$  over the range of  $C_{salt}$  between 0.15 and 1.2 M indicating that the hydrophobic associations are so strong that they are not destroyed during the expansion of the gel network in water.

The swelling kinetics of the physical gels in water is shown by the filled symbols in Figure 5B. Because of the osmotic pressure of SDS counterions inside the gel network, the gel initially behaves like an ionic gel and thus exhibits a large swelling ratio  $m_{rel}$ . However, as SDS is progressively extracted from the gel network, the osmotic effect disappears and the gel gradually converts into a nonionic gel having a markedly reduced swelling ratio ( $1.3 \pm 0.3$  for  $C_{salt} = 0.2$ – $0.8$  M). Indeed, SDS concentration in the external solutions (before refreshing) rapidly dropped below the detection limit of the methylene blue method ( $0.20$  mg·L<sup>-1</sup>) after 10 d. This

interpretation of the course of the swelling curves was confirmed by conducting swelling tests in aqueous NaCl solutions (open symbols in Figure 5B). The addition of salt into the external solution decreases the swelling ratios at short times because the osmotic pressure difference between inside and outside of the gel is reduced. As the NaCl concentration in the solution approaches to the counterion concentration in the gel (0.74 M), the maximum of the swelling curves entirely disappears.

Swelling of the gels in SDS solutions exhibits a strikingly different behavior (Figure 5C). In solutions below 5 w/v % SDS, the preferential absorption of SDS by the polymer network produces an excess counterion concentration inside the gel and leads to increased gel swelling.<sup>60,61</sup> However, at higher SDS content, it was found that all of the hydrogels dissolve within 3 to 5 days. This observation indicates that an excess of SDS solubilizes the hydrophobic blocks so that the physical cross-links can dissociate. The physical nature of the cross-links in these hydrogels is thus clearly substantiated. An interesting property of the polymer isolated from the dissolved gel networks is their insolubility in water, even at high temperatures, but their solubility in SDS micellar solutions. Although the hydrophobic part is only a small fraction of the polymer chains (2 mol %), this swelling feature is in agreement with previous reports on hydrophobically modified polyacrylamides<sup>19</sup> and indicates the blocky structure of the network chains. FTIR spectra of the polymers

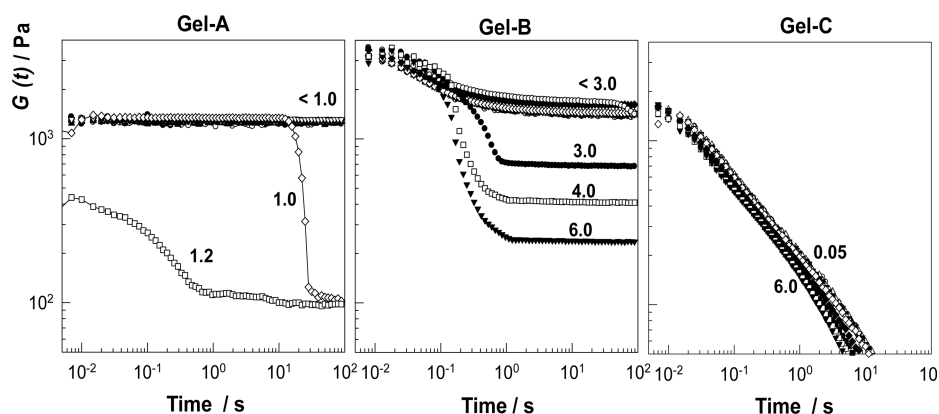


**Figure 6.** The relaxation modulus  $G(t)$  as a function of time  $t$  for various strains  $\gamma_o$  indicated. SDS = 7 w/v %. The gels were prepared in 0.5 M NaCl with BAAM (Gel-A), with BAAM + C18 (Gel-B), and with only C18 (Gel-C).

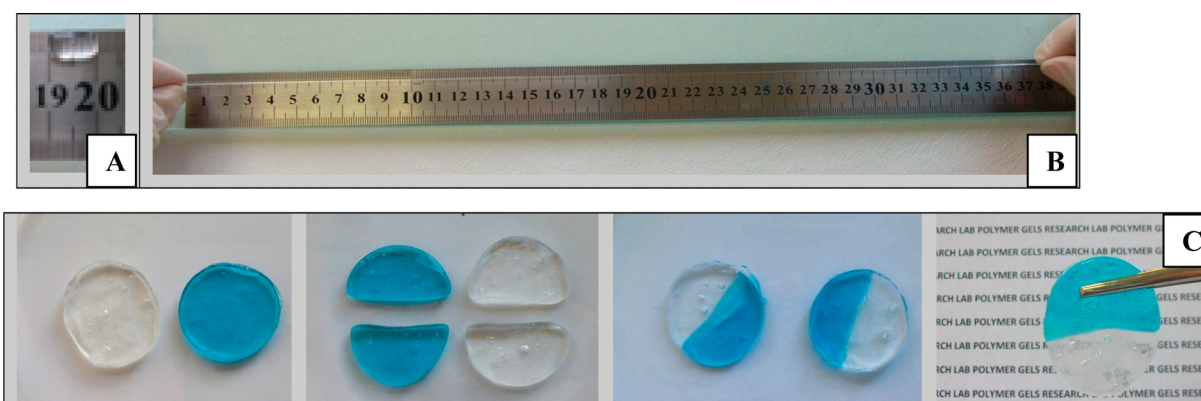


**Figure 7.** Photographs before (A) and after stretching of a hydrogel sample formed in 0.5 M NaCl (B). (C) Photographs of two hydrogel samples formed in 0.5 M NaCl. One of the gel samples is colored with methylene blue for clarity. After cutting into two pieces and pressing the fractured surfaces together, they merge into a single piece.

show the characteristic bands at 2920 and 2852  $\text{cm}^{-1}$  due to the stretching of the methylene groups of C18 units (Figure S4, Supporting Information).

**Physical vs Chemical PAAm Gels.** In order to compare the rheological properties of hydrogels formed using C18 with conventional, covalently cross-linked hydrogels, three types of gels were prepared in 0.5 M NaCl solutions of SDS:

- (i) Conventional PAAm gel with BAAM cross-linker at a cross-linker ratio  $X = 1/80$  (Gel-A),
- (ii) PAAm gel containing both the chemical cross-linker BAAM at  $X = 1/80$  and 2 mol % C18 (Gel-B), and
- (iii) PAAm gel with only 2 mol % C18 (Gel-C).

The gels were subjected to stress relaxation measurements. Figure 6 shows the relaxation modulus  $G(t)$  at different strains  $\gamma_o$  as a function of time  $t$ . The chemically cross-linked gel prepared with BAAM cross-linker (Gel-A) exhibits a time independent modulus and breaks at about 100% strain. However, with the incorporation of hydrophobic blocks into the covalently cross-linked network (Gel-B), the modulus increases markedly at short times due to the hydrophobic associations acting as additional, temporary cross-links. This additional contribution relaxes on a time scale of seconds. (The data at very short times,  $t < 0.03$  s, should be taken with care due to the response time of the rheometer.) Gel-B seems to be in the linear regime for  $\gamma_o \leq 1$ . At higher strains, the short-time behavior ( $t < 0.1$  s) remains

essentially unchanged, while there is a drastic and nonlinear relaxation occurring between 0.1 and a few seconds. This is probably due to the partial breakdown of the permanent network. Interestingly, the long-time modulus, which is decreasing with rising strain, remains on a markedly higher level than that of gel A. If the gel contains only physical cross-links (Gel-C), the modulus decreases significantly with time indicating the temporary nature of the hydrophobic associations having lifetimes of the order of seconds. This behavior observed here at large strains up to 6, agrees fully with the frequency dependence of the small-strain storage modulus (Figure 4B). Figure 6 thus reveals that the finite lifetime of hydrophobic associations between C18 blocks leads to the formation of gels with a high degree of toughness.

The toughness of the physical gels was also tested by tensile mechanical measurements. Hydrogels were mechanically stable up to very large extension ratios. However, due to the weakness of the gels, precise mechanical data could not be obtained even by use of a load cell of 10 N. Therefore, cylindrical gel samples of 5 mm in diameter and 6 cm in length were firmly stretched by hand to record the elongation ratio at break. For gels formed in 0.5 M NaCl, an average elongation ratio at break of  $3600 \pm 630\%$  was recorded at 20 °C (Figure 7). Considering the fact that the chemical PAAm hydrogels prepared under the same experimental conditions break at a few ten percent elongation, the results demonstrate the extraordinary mechanical behavior of the present

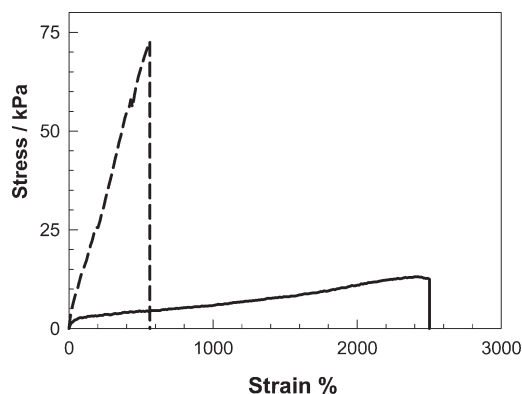


**Figure 8.** Stress–strain curves of C18 hydrogels after preparation (solid curve) and after equilibrium swelling in water (dashed curve). C18 = 2 mol %. Initial monomer concentration = 9 w/v %.

gels. This is due to the reversible disengagements of the hydrophobic units from the associations, which dissipate the crack energy along the sample and prevent the crack propagation.

The reversible dissociation–association of the cross-link zones in the gel network also provides self-healing property to the present hydrogels. As illustrated in Figure 7, when the fracture surfaces of a ruptured gel sample are pressed together, the two pieces merge into a single piece. The joint reformed withstands very large extension ratios as the original gel sample before its fracture. To quantify the extent of healing in the physical gels, 14 cylindrical gel samples of 5 mm in diameter and 6 cm in length were subjected to elongation tests with hand. Before the tests, 7 gel samples were cut in the middle and then the two halves were merge together into a single piece by pressing slightly for a few seconds without changing the original shape and diameter. The original and healed gel samples broke at elongation ratios of  $3600 \pm 630$  and  $3580 \pm 520\%$ , respectively, indicating a healing efficiency of about 100%. The self-healing performance of the hydrogels formed using C18 is also illustrated in the attached movie.

We should note that all the mechanical tests reported above were conducted on hydrogel samples just after their preparation so that they contain surfactant molecules and micelles. Although extracted swollen hydrogels formed between  $C_{salt} = 0.2$  and 0.8 M exhibit an average modulus of elasticity ( $G_{swollen}$ ) of  $1 \pm 0.2$  kPa, similar to the modulus of the unextracted samples, they are fragile and do not exhibit the extraordinary mechanical performance. This is attributed to the effect of SDS on the stability of the physical cross-links. When SDS micelles are present, the hydrophobic moieties of the network chains can be solubilized so that the associations are weakened and become reversible, while with no SDS present (after extraction), the associations are so strong that the gel behaves mostly like being covalently cross-linked. The mechanical properties, in particular the relaxation behavior and the self-healing properties, can thus be controlled by the amount of surfactant present in the system.

To verify this hypothesis, hydrogels were prepared under the same experimental condition but at a higher monomer concentration (9 w/v %) so that mechanical tests using Zwick test machine could be conducted. Figure 8 represents tensile stress–strain data of the hydrogels after preparation (solid curve) and after equilibrium swelling in water (dashed curve). The tensile strength of the gel, which was originally  $12 \pm 1$  kPa, increased to  $78 \pm 6$  kPa after equilibrium swelling in water ( $m_{rel} = 1.3$ ). Simultaneously, the

elongation ratio at break decreased from  $2200 \pm 350\%$  to  $650 \pm 80\%$ , indicating an increased stiffness of the physical gels after extraction of SDS micelles. These results also explain the insolubility of the present self-healing hydrogels in water.

Experiments were repeated by replacing C18 with a more hydrophobic comonomer, namely with dococyl acrylate (C22) having an alkyl chain length of 22 carbons. Dynamic moduli vs reaction time profiles of the micellar copolymerization of AAm and C22 were similar to those given in Figure 3 (Figure S5, Supporting Information). The limiting values of the dynamic moduli do not change much up to 0.10 M NaCl while they increase rapidly at higher salt contents. The loss factor  $\tan \delta$  decreases below unity at 0.3 M NaCl, as compared to 0.10 M obtained using the hydrophobe C18, indicating that a larger amount of salt is required for the formation of a viscoelastic gel. The critical salt concentration  $C_{salt}$ , where the loss tangent is frequency independent, shifts from 0.15 to 0.60 M by replacing C18 with C22 monomer (Figure S6, Supporting Information). Hydrogels with a gel fraction  $W_g = 0.95 \pm 0.01$  could be obtained at or above  $C_{salt} = 0.60$  M. The tensile tests conducted on the hydrogel samples gave an elongation ratio at break of 1300–1700% at 1.2–2.7 kPa (Figure S7, Supporting Information). We have to note that the gels formed using C22 exhibit increasing elasticity with increasing salt concentration and, they do not show any self-healing ability. However, C18 gels are in a state close to the critical gel state over a wide range of  $C_{salt}$ . This reveals that many free C18 blocks are present in C18 hydrogels that are not participated into hydrophobic associations. As a consequence, the free, nonassociated C18 blocks locating near the fracture surface of the gel samples link each other to self-heal the broken hydrogels.

## CONCLUSION

Acrylamide could be copolymerized with large hydrophobes such as C18 or C22 in a micellar system provided that an electrolyte, such as NaCl, has been added in sufficient amount. Increasing NaCl content in the reaction solution causes micellar growth, solubilization of the hydrophobes within the micelles and thus, incorporation of the hydrophobic comonomer in the form of blocks within the PAAm chains. Hydrogels with gel fractions around 0.9 were obtained at or above  $C_{salt} = 0.15$  and 0.60 M NaCl, for C18 and C22, respectively, indicating that the hydrophobic associations are so strong that they are not destroyed during the expansion of the gel network in water. The gels exhibit unusual swelling kinetics in water and, they can only be dissolved in SDS solutions demonstrating the physical nature of cross-links. Hydrogels exhibit an elastic modulus  $G'$  at 1 Hz of around 1 kPa and a loss factor of 0.5–0.9. Both  $G'$  and  $G''$  of C18 hydrogels formed between  $C_{salt} = 0.24$ –0.80 are congruent showing power-law behavior,  $G' \propto \omega^{0.46 \pm 0.03}$ ,  $G'' \propto \omega^{0.44 \pm 0.01}$ , which suggests that the gels are close to the critical gel state possessing self-similar fractal structure over a wide spatial scale. The hydrogels are more homogeneous than the corresponding chemical PAAm hydrogel due to the mobility of the cross-link zones. The finite lifetime of hydrophobic associations between C18 or C22 blocks also leads to the formation of gels with a high degree of toughness. Mechanical tests indeed show that C18 and C22 hydrogel samples broke at elongation ratios of 3600% and 1300–1700%, respectively. Dynamic nature of the junction zones between the network chains in C18 hydrogels provides a self-healing efficiency to elongation at break of about 100%.

## ■ ASSOCIATED CONTENT

**S Supporting Information.** Figure S1, the decomposition plots according to eq 4; Figure S2, the hydrodynamic correlation length of SDS solutions; Figure S3, the intensity time correlation functions of gels and solutions; Figure S4, the FTIR spectrum of the polymer isolated from the hydrogel network; Figure S5, the dynamic moduli versus reaction time profiles of the micellar copolymerization of AAm and C22; Figure S6, the results of the frequency sweep tests conducted on C22 hydrogels and the exponents of  $G'$  and  $G''$  vs frequency plots; and Figure S7, the stress–strain curves of C22 hydrogels. This material is available free of charge via the Internet at <http://pubs.acs.org>.

## ■ ACKNOWLEDGMENT

Work was supported by the Scientific and Technical Research Council of Turkey (TUBITAK) and International Bureau of the Federal Ministry of Education and Research of Germany (BMBF), TBAG –109T646. O.O. thanks the Turkish Academy of Sciences (TUBA) for partial support.

## ■ REFERENCES

- (1) Fratzl, P. *J. R. Soc. Interface* **2007**, *4*, 637.
- (2) Amendola, V.; Meneghetti, M. *Nanoscale* **2009**, *1*, 74.
- (3) Fantner, G. E.; Oroudjev, E.; Schitter, G.; Golde, L. S.; Thurner, P.; Finch, M. M.; Turner, P.; Gutschmann, T.; Morse, D. E.; Hansma, H.; Hansma, P. K. *Biophys. J.* **2006**, *90*, 1411.
- (4) Gong, J. P.; Katsuyama, Y.; Kurokawa, T.; Osada, Y. *Adv. Mater.* **2003**, *15*, 1155.
- (5) Tanaka, Y.; Gong, J. P.; Osada, Y. *Prog. Polym. Sci.* **2005**, *30*, 1.
- (6) Okumura, Y.; Ito, K. *Adv. Mater.* **2001**, *13*, 485.
- (7) Miquelard-Garnier, G.; Demoures, S.; Creton, C.; Hourdet, D. *Macromolecules* **2006**, *39*, 8128.
- (8) Haraguchi, K.; Takehisa, T. *Adv. Mater.* **2002**, *14*, 1120.
- (9) Huang, T.; Xu, H.; Jiao, K.; Zhu, L.; Brown, H. R.; Wang, H. *Adv. Mater.* **2007**, *19*, 1622.
- (10) Deng, G.; Tang, C.; Li, F.; Jiang, H.; Chen, Y. *Macromolecules* **2010**, *43*, 1191.
- (11) Ahagon, A.; Gent, A. N. *J. Polym. Sci., Polym. Phys. Ed.* **1975**, *13*, 1903.
- (12) Brown, H. R. *Macromolecules* **2007**, *40*, 3815.
- (13) Abdurrahmanoglu, S.; Can, V.; Okay, O. *Polymer* **2009**, *50*, 5449.
- (14) Cordier, P.; Tournilhac, F.; Souli-Ziakovic, C.; Leibler, L. *Nature* **2008**, *451*, 977.
- (15) Wu, D. Y.; Meure, S.; Solomon, D. *Prog. Polym. Sci.* **2008**, *33*, 479.
- (16) Wietor, J.-L.; Dimopoulos, A.; Govaert, L. E.; van Benthem, R. A. T. M.; de With, G.; Sijbesma, R. P. *Macromolecules* **2009**, *42*, 6640.
- (17) Skrzyszewska, P. J.; Sprakel, J.; Wolf, F. A.; Fokink, R.; Stuart, M. A. C.; van de Gucht, J. *Macromolecules* **2010**, *43*, 3542.
- (18) Shibayama, M.; Tanaka, T. *Adv. Polym. Sci.* **1993**, *109*, 1.
- (19) Hill, A.; Candau, F.; Selb, J. *Macromolecules* **1993**, *26*, 4521.
- (20) Volpert, E.; Selb, J.; Françoise, C. *Polymer* **1998**, *39*, 1025.
- (21) Regalado, E. J.; Selb, J.; Candau, F. *Macromolecules* **1999**, *32*, 8580.
- (22) Candau, F.; Selb, J. *Adv. Colloid Interface Sci.* **1999**, *79*, 149.
- (23) Gao, B.; Guo, H.; Wang, J.; Zhang, Y. *Macromolecules* **2008**, *41*, 2890.
- (24) Candau, F.; Regalado, E. J.; Selb, J. *Macromolecules* **1998**, *31*, 5550.
- (25) Kujawa, P.; Audibert-Hayet, A.; Selb, J.; Candau, F. *J. Polym. Sci., Part B: Polym. Phys.* **2004**, *42*, 1640.
- (26) Kujawa, P.; Audibert-Hayet, A.; Selb, J.; Candau, F. *Macromolecules* **2006**, *39*, 384.
- (27) Abdurrahmanoglu, S.; Cilingir, M.; Okay, O. *Polymer* **2011**, *52*, 694.
- (28) Chern, C. S.; Chen, T. J. *Colloids Surf. A: Physicochem. Eng. Aspects* **1998**, *138*, 65.
- (29) Leyrer, R. J.; Machtle, W. *Macromol. Chem. Phys.* **2000**, *201*, 1235.
- (30) Lau, W. *Macromol. Symp.* **2002**, *182*, 283.
- (31) Rehage, H.; Hoffman, H. *Mol. Phys.* **1991**, *74*, 933.
- (32) (a) Magid, L. J. *J. Phys. Chem. B* **1998**, *102*, 4064. (b) Hassan, P. A.; Raghavan, S. R.; Kaler, E. W. *Langmuir* **2002**, *18*, 2543. (c) Missel, P. J.; Mazer, N. A.; Benedek, G. B.; Young, C. Y. *J. Phys. Chem.* **1980**, *84*, 1044. (d) Sutherland, E.; Mercer, S. M.; Everist, M.; Leaist, D. *J. Chem. Eng. Data* **2009**, *54*, 272.
- (33) Cates, M. E.; Candau, S. J. *J. Phys.: Condens. Matter* **1990**, *2*, 6869.
- (34) Mazer, N. A.; Benedek, G. B.; Carey, M. C. *J. Phys. Chem.* **1976**, *80*, 1075.
- (35) Corti, M.; Degiorgio, V. *J. Phys. Chem.* **1981**, *85*, 711.
- (36) Young, C. Y.; Missel, P. J.; Mazer, N. A.; Benedek, G. B.; Carey, M. C. *J. Phys. Chem.* **1978**, *82*, 1375.
- (37) Ikeda, S.; Hayashi, S.; Imae, T. *J. Phys. Chem.* **1981**, *85*, 106.
- (38) Zhao, J.; Fung, B. M. *Langmuir* **1993**, *9*, 1228.
- (39) Magid, L. J.; Li, Z.; Butler, P. D. *Langmuir* **2000**, *16*, 10028.
- (40) Hayashi, S.; Ikeda, S. *J. Phys. Chem.* **1980**, *84*, 744.
- (41) Molchanov, V. S.; Philippova, O. E.; Khokhlov, A. R.; Kovalev, Y. A.; Kuklin, A. I. *Langmuir* **2007**, *23*, 105.
- (42) Kumar, S.; Bansal, D.; Din, K. *Langmuir* **1999**, *15*, 4960.
- (43) Kunieda, H.; Ozawa, K.; Huang, K.-L. *J. Phys. Chem. B* **1998**, *102*, 831.
- (44) Siriawatwechakul, W.; LaFleur, T.; Prud'homme, R. K.; Sullivan, P. *Langmuir* **2004**, *20*, 8970.
- (45) Miyazaki, T.; Kaneko, T.; Gong, J. P.; Osada, Y. *Macromolecules* **2001**, *34*, 6024.
- (46) Joosten, J. G. H.; McCarthy, J. L.; Pusey, P. N. *Macromolecules* **1991**, *24*, 6690–6699.
- (47) Pusey, P. N.; van Meegen, W. *Physica A* **1989**, *157*, 705–741.
- (48) Ikkai, F.; Shibayama, M. *Phys. Rev. Lett.* **1999**, *82*, 4946–4949.
- (49) ISO 7875-1, 1996. Water quality. Determination of surfactants. Part 1: Determination of anionic surfactants by measurement of the methylene blue index (MBAS). ISO/TC 147.
- (50) Gundogan, N.; Melekaslan, D.; Okay, O. *Macromolecules* **2002**, *35*, 5616.
- (51) Collura, J. S.; Harrison, D. E.; Richards, C. J.; Kole, T. K.; Fisch, M. R. *J. Phys. Chem. B* **2001**, *105*, 4846.
- (52) Pecora, R. *Dynamic Light Scattering: Application of Photon Correlation Spectroscopy*; Plenum Press: New York, 1985.
- (53) For prolate ellipsoids, the radius  $\xi_H$  is related to the semimajor axis  $a$  of the micelles by  $\xi_H = a / G(\rho)$ , where  $G(\rho) = (1 - \rho^2)^{-0.5} \ln \{ \rho^{-1} [1 + (1 - \rho^2)^{0.5}] \}$  and  $\rho$  is the ratio of semiminor axis  $b$  to the semimajor axis  $a$  ( $\rho < 1$ ). The aggregation number  $N_{agg}$  relates to the axis ratio by  $N_{agg} = N_{agg,0} / \rho^{34}$ , where  $N_{agg,0}$  is the aggregation number of the minimum spherical micelle.<sup>60</sup>
- (54) Sato, T.; Acharya, D. P.; Kaneko, M.; Aramaki, K.; Singh, Y.; Ishitobi, M.; Kunieda, H. *J. Disp. Sci. Technol.* **2006**, *27*, 611.
- (55) Karino, T.; Okumura, Y.; Ito, K.; Shibayama, M. *Macromolecules* **2004**, *37*, 6177.
- (56) Karino, T.; Shibayama, M.; Ito, K. *Physica B* **2006**, *385–386*, 692.
- (57) Nie, J.; Du, B.; Oppermann, W. *J. Phys. Chem. B* **2006**, *110*, 11167.
- (58) Winter, H. H.; Chambon, F. *J. Rheol.* **1986**, *30*, 367.
- (59) Chambon, F.; Winter, H. H. *J. Rheol.* **1987**, *31*, 683.
- (60) Philippova, O. E.; Hourdet, D.; Audebert, R.; Khokhlov, A. R. *Macromolecules* **1996**, *29*, 2822.
- (61) Kokufuta, E.; Nakaizumi, S.; Ito, S.; Tanaka, T. *Macromolecules* **1993**, *26*, 1053.